World Academy of Science, Engineering and Technology
International Journal of Civil and Environmental Engineering
Vol:14, No:7, 2020

Dynamic Interaction between Two Neighboring Tunnels in a Layered Half-Space

Chao He, Shunhua Zhou, Peijun Guo

***Abstract*—**The vast majority of existing underground railway lines consist of twin tunnels. In this paper, the dynamic interaction between two neighboring tunnels in a layered half-space is investigated by an analytical model. The two tunnels are modelled as cylindrical thin shells, while the soil in the form of a layered half-space with two cylindrical cavities is simulated by the elastic continuum theory. The transfer matrix method is first used to derive the relationship between the plane wave vectors in arbitrary layers and the source layer. Thereafter, the wave translation and transformation are introduced to determine the plane and cylindrical wave vectors in the source layer. The solution for the dynamic interaction between twin tunnels in a layered half-space is obtained by means of the compatibility of displacements and equilibrium of stresses on the two tunnel–soil interfaces. By coupling the proposed model with a fully track model, the train-induced vibrations from twin tunnels in a multi-layered half-space are investigated. The numerical results demonstrate that the existence of a neighboring tunnel has a significant effect on ground vibrations.

***Keywords*—**Underground railway, twin tunnels, wave translation and transformation, transfer matrix method.

I. Introduction

MANY underground railway lines have been constructed to alleviate the urban traffic congestion. Comparing to the road traffic, the underground railway has many advantages, such as efficiency, energy conservation, safety and comfort. However, ground-borne noise and vibrations induced by underground railway traffic have been recognized as an important environmental issue. Owing to wheel and track irregularities, vibrations generated at the wheel-rail interface propagate to adjacent buildings, which may annoy the surrounding residents. Therefore, it is necessary to develop an accurate and efficient model for designers to predict the vibration levels induced by underground railways.

With the improvement of calculation ability, some numerical models have been established to compute train-induced vibrations from underground tunnels, such as the periodic FE–BE method [1]-[3], two-and-a-half-dimensional (2.5D) coupled FE–BE method [4]-[8], 2.5D finite/infinite element method [8]-[10].

As an alternative to the numerical methods, the analytical methods have the advantage of high computational efficiency. For example, the pipe-in-pipe (PiP) model developed by [11], [12] is an analytical approach with high computational efficiency. Hussein et al. [13] extend this model to consider the influence of the ground surface and layer interfaces, while [14], [15] advanced their results to investigate the influence of pore water in soils. He et al. [16] recently proposed an analytical model to predict vibrations from a tunnel in layered half-space by using the wave transformation and transfer matrix method.

It should be noted that only one tunnel was considered in the above studies. However, most underground railway lines around the world consist of twin tunnels, used for the outbound and inbound directions, respectively. Based on the PiP mode, [17] proposed a superposition model to calculate ground vibrations from twin tunnels in a homogeneous full-space. Based on the BE method, [18] established the superposition and fully coupled models to compute ground vibrations from twin tunnels in a homogeneous half-space. However, the discretization of the tunnel-soil interfaces is required in those models, which increases computational efforts. He et al. [19] recently proposed an analytical model to analyze the effect of the dynamic interaction between twin tunnels in a full-space. A virtual interface along with the transformation between plane and cylindrical waves was introduced to address the dynamic interaction between twin tunnels. However, this model cannot be applied to the layered half-space because the infinitely long virtual interface will be cut off by the ground surface and layer interfaces.

This paper develops an efficient analytical model for predicting the ground vibrations from twin tunnels in a layered half-space. To solve the problem of multiple scattering of waves induced by the two cylindrical cavities, layer interfaces and ground surface, the transfer matrix method is first used to deal with wave propagation in layered medium. By using the translation between two different cylindrical waves and transformation between plane and cylindrical waves, the solution for the dynamic interaction between two neighboring tunnels in a layered half-space is obtained by means of the continuous conditions at the tunnel–soil interfaces.

II. Governing Equations and General Solutions

As illustrated in Fig. 1, the $Q + 1$ soil layers with an infinite domain are simulated as a 3D isotropic elastic solid. The two parallel tunnels are embedded in the S-th layer (source layer). The subscripts R and L represent the tunnels on the right-hand side (Tunnel 1) and left-hand side (Tunnel 2), respectively. The twin tunnels are separated by a distance d_t, with Tunnel 2 located at an angle θ_t from Tunnel 1. Two cylindrical coordinate systems, (r_R, θ_R, z) and (r_L, θ_L, z), are centered on

Chao He and Peijun Guo are with the Department of Civil Engineering, McMaster University, Hamilton, ON L8S 4L7, Canada, (e-mail: chaohe1990@gmail.com, guop@mcmaster.ca).

Shunhua Zhou is with the Shanghai Key Laboratory of Rail Infrastructure Durability and System Safety, Tongji University, Shanghai, 201804, China, (e-mail: zhoushh@tongji.edu.cn).

Tunnels 1 and 2, respectively, and oriented clockwise. Two corresponding Cartesian coordinate systems, (x_R, y_R, z) and (x_L, y_L, z), are also defined at the same origins. Moreover, $x_{(q)}$ denotes the local vertical coordinate of the soil layer L_q. The origin of $x_{(q)}$ for the layer above the source layer ($q < S$) begins from its lower interface, while it begins from its upper interface for the layer under the source layer ($q > S$).

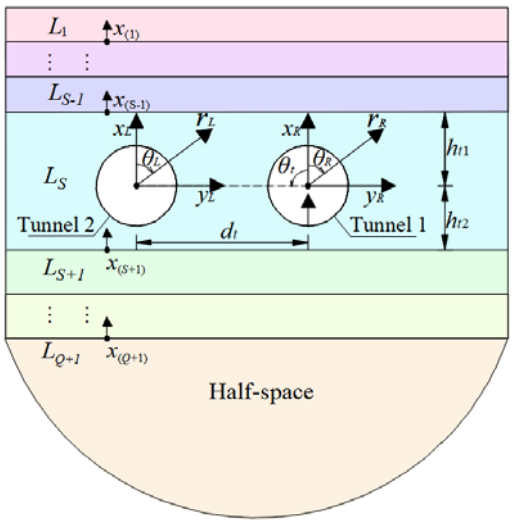

Fig. 1 3D geometry of twin tunnels embedded in a multi-layered half-space

The basic assumption underlying in this modelling process is that the geometries of the twin tunnels and soil are longitudinally invariant. Therefore, the proposed model can be derived in the frequency and wavenumber domains via the following Fourier transforms [20]:

$$\hat{\tilde{f}}(k_z,\omega)=\int_{-\infty}^{+\infty}\int_{-\infty}^{+\infty} f(z,t)\mathrm{e}^{\mathrm{i}(k_z z+\omega t)}\mathrm{d}z\mathrm{d}t \tag{1}$$

The transfer matrix method developed by [21] and [22] is introduced to derive the solution for wave propagation in the multi-layered soil. Since the main derivation process is similar to that in [16], only a brief introduction is presented here. If the tunnel is not situated at the q-th layer (i.e. $q \neq S$), the displacement and stress components can be expressed in the frequency–double wavenumber domain as:

$$\begin{aligned}\hat{\tilde{\boldsymbol{\Omega}}}^{(q)}(x_{(q)},k_y,k_z,\omega)&=\left[\hat{\tilde{u}}_x^{(q)}\quad \hat{\tilde{u}}_y^{(q)}\quad \hat{\tilde{u}}_z^{(q)}\quad \hat{\tilde{\sigma}}_{xx}^{(q)}\quad \hat{\tilde{\sigma}}_{xy}^{(q)}\quad \hat{\tilde{\sigma}}_{xz}^{(q)}\right]^{\mathrm{T}}\\&=\begin{bmatrix}\mathbf{D}_d^{(q)}(k_y,k_z,\omega) & \mathbf{D}_u^{(q)}(k_y,k_z,\omega)\\ \mathbf{S}_d^{(q)}(k_y,k_z,\omega) & \mathbf{S}_u^{(q)}(k_y,k_z,\omega)\end{bmatrix}\begin{bmatrix}\mathbf{E}_d^{(q)}(x_{(q)}) & \mathbf{0}\\ \mathbf{0} & \mathbf{E}_u^{(q)}(x_{(q)})\end{bmatrix}\begin{bmatrix}\mathbf{A}_d^{(q)}\\ \mathbf{A}_u^{(q)}\end{bmatrix}\end{aligned} \tag{2}$$

where the expressions of the sub-matrixes $\mathbf{D}_d^{(q)}$, $\mathbf{D}_u^{(q)}$, $\mathbf{S}_d^{(q)}$, $\mathbf{S}_u^{(q)}$, $\mathbf{E}_d^{(q)}$, and $\mathbf{E}_u^{(q)}$ are provided in Appendix A. $\mathbf{A}_d^{(q)}=\left[A_{d1}^{(q)}\quad A_{d2}^{(q)}\quad A_{d3}^{(q)}\right]^{\mathrm{T}}$ and $\mathbf{A}_u^{(q)}=\left[A_{u1}^{(q)}\quad A_{u2}^{(q)}\quad A_{u3}^{(q)}\right]^{\mathrm{T}}$ represent the unknown coefficient vectors associated with the down- and up-going plane waves, respectively, in the layer L_q.

According to the transfer matrix method [16], the unknown coefficient vectors $\mathbf{A}_d^{(S-1)}$ and $\mathbf{A}_u^{(S-1)}$ in L_{S-1} are related via:

$$\begin{aligned}\mathbf{A}_d^{(S-1)}=&-(\mathbf{R}_d\mathbf{T}_{d21}^{(1)}-\mathbf{T}_{d11}^{(1)})^{-1}\\&\times(\mathbf{R}_d\mathbf{T}_{d22}^{(1)}-\mathbf{T}_{d12}^{(1)})\mathbf{A}_u^{(S-1)}=\mathbf{Q}_d\mathbf{A}_u^{(S-1)}\end{aligned} \tag{3}$$

with

$$\mathbf{R}_d=-\left[\mathbf{S}_d^{(1)}\mathbf{E}_d^{(1)}(h_1)\right]^{-1}\mathbf{S}_u^{(1)}\mathbf{E}_u^{(1)}(h_1) \tag{4}$$

Similarly, the unknown coefficient vectors $\mathbf{A}_d^{(S+1)}$ and $\mathbf{A}_u^{(S+1)}$ in L_{S+1} are related via:

$$\mathbf{A}_d^{(S+1)}=-\left[\mathbf{T}_{u21}^{(Q+1)}\right]^{-1}\mathbf{T}_{u22}^{(Q+1)}\mathbf{A}_u^{(S+1)}=\mathbf{Q}_u\mathbf{A}_u^{(S+1)} \tag{5}$$

where the expressions of the sub-matrixes $\mathbf{T}_{dij}^{(q)}$ and $\mathbf{T}_{uij}^{(q)}$ are provided in [16].

A. Solution for the Source Layer

The total wave field in the source layer L_S consists of the down- and up-going plane waves and two types of outgoing cylindrical waves. Therefore, the displacement and stress components in L_S are expressed in the frequency–wavenumber domain as:

$$\begin{aligned}\hat{\tilde{\mathbf{u}}}^{(S)}=&\frac{1}{2\pi}\int_{-\infty}^{+\infty}\sum_{j=1}^{3}\left[A_{dj}^{(S)}\hat{\tilde{\boldsymbol{\phi}}}_{dj}^{(S)}(x_R,k_y,k_z,\omega)+A_{uj}^{(S)}\hat{\tilde{\boldsymbol{\phi}}}_{uj}^{(S)}(x_R,k_y,k_z,\omega)\right]\mathrm{d}k_y\\&+\sum_{n=-N}^{N}\sum_{j=1}^{3}\left[B_{nj}^{R}\hat{\boldsymbol{\chi}}_{nj}^{R}(r_R,\theta_R,k_z,\omega)+B_{nj}^{L}\hat{\boldsymbol{\chi}}_{nj}^{L}(r_L,\theta_L,k_z,\omega)\right]\end{aligned} \tag{6a}$$

$$\begin{aligned}\hat{\tilde{\boldsymbol{\sigma}}}^{(S)}=&\frac{1}{2\pi}\int_{-\infty}^{+\infty}\sum_{j=1}^{3}\left[A_{dj}^{(S)}\hat{\tilde{\boldsymbol{\Psi}}}_{dj}^{(S)}(x_R,k_y,k_z,\omega)+A_{uj}^{(S)}\hat{\tilde{\boldsymbol{\Psi}}}_{uj}^{(S)}(x_R,k_y,k_z,\omega)\right]\mathrm{d}k_y\\&+\sum_{n=-N}^{N}\sum_{j=1}^{3}\left[B_{nj}^{R}\hat{\boldsymbol{\eta}}_{nj}^{R}(r_R,\theta_R,k_z,\omega)+B_{nj}^{L}\hat{\boldsymbol{\eta}}_{nj}^{L}(r_L,\theta_L,k_z,\omega)\right]\end{aligned} \tag{6b}$$

where the expressions of the wave functions $\hat{\tilde{\boldsymbol{\phi}}}_{dj}^{(S)}$, $\hat{\tilde{\boldsymbol{\phi}}}_{uj}^{(S)}$, $\hat{\tilde{\boldsymbol{\Psi}}}_{dj}^{(S)}$, $\hat{\tilde{\boldsymbol{\Psi}}}_{uj}^{(S)}$, $\hat{\tilde{\boldsymbol{\chi}}}_{nj}^{R,L}$, and $\hat{\boldsymbol{\eta}}_{nj}^{R,L}$ are provided in [19]. Furthermore, $B_{nj}^{R,L}$ represents the unknown coefficients corresponding to those outgoing cylindrical waves.

In order to handle the continuity conditions on the upper and lower interfaces of the source layer L_S, the outgoing cylindrical wave functions need to be expressed in the Cartesian coordinate system. By introducing the integral representations of the Hankel function of the first kind [23], those cylindrical waves in L_S can be transformed into the down- and up-going plane waves, as follows:

$$\begin{aligned}\tilde{\boldsymbol{\chi}}_{nj}^{R,L}(r_{R,L},\theta_{R,L})&=\frac{1}{2\pi}\int_{-\infty}^{+\infty}2T_{unj}^{R,L}\hat{\tilde{\boldsymbol{\phi}}}_{uj}^{(S)}(x_R,k_y)/k_{xj}^{(S)}\mathrm{d}k_y,\quad x_R>0\\\tilde{\boldsymbol{\chi}}_{nj}^{R,L}(r_{R,L},\theta_{R,L})&=\frac{1}{2\pi}\int_{-\infty}^{+\infty}2T_{dnj}^{R,L}\hat{\tilde{\boldsymbol{\phi}}}_{dj}^{(S)}(x_R,k_y)/k_{xj}^{(S)}\mathrm{d}k_y,\quad x_R<0\end{aligned} \tag{7}$$

where $k_{xj}^{(S)}=k_{xs}^{(S)}$ for $j=1, 2$ and $k_{xj}^{(S)}=k_{xp}^{(S)}$ for $j=3$, with

$$
\begin{aligned}
&T_{unj}^{R}=\mathrm{i}^{-n}\begin{cases}\mathrm{e}^{\mathrm{i}n\beta_s^{(S)}}\\ \mathrm{e}^{\mathrm{i}n\beta_p^{(S)}}\end{cases},\ T_{dnj}^{R}=\mathrm{i}^{n}\begin{cases}\mathrm{e}^{-\mathrm{i}n\beta_s^{(S)}}, j=1,2\\ \mathrm{e}^{-\mathrm{i}n\beta_p^{(S)}},\ j=3\end{cases}\\
&\beta_s^{(S)}=\arcsin(k_y/k_{rs}^{(S)}),\ \beta_p^{(S)}=\arcsin(k_y/k_{rp}^{(S)}),\\
&T_{unj}^{L}=T_{unj}^{R}\mathrm{e}^{\mathrm{i}(-k_{xj}^{(S)}d_t\cos\theta_t+k_yd_t\sin\theta_t)},\ T_{dnj}^{L}=T_{dnj}^{R}\mathrm{e}^{\mathrm{i}(-k_{xj}^{(S)}d_t\cos\theta_t+k_yd_t\sin\theta_t)}
\end{aligned}
\tag{8}
$$

By substituting (7) into (6), the displacement and stress components in L_S can be expressed in the Cartesian coordinate system (x_R, y_R, z). Thereafter, by applying the continuity conditions on the upper ($x_R = h_{t1}$) and lower ($x_R = -h_{t2}$) interfaces of L_S, the unknown coefficients $A_{dj}^{(S)}$ and $A_{uj}^{(S)}$ can be expressed in terms of $B_{nj}^{R,L}$:

$$
\begin{aligned}
A_{dj}^{(S)}&=\sum_{j'=1}^{3}\sum_{n=-N}^{N}(L_{djnj'}^{R}B_{nj'}^{R}+L_{djnj'}^{L}B_{nj'}^{L}),\\
A_{uj}^{(S)}&=\sum_{j'=1}^{3}\sum_{n=-N}^{N}(L_{ujnj'}^{R}B_{nj'}^{R}+L_{ujnj'}^{L}B_{nj'}^{L})
\end{aligned}
\tag{9}
$$

with

$$
\begin{aligned}
&\left[L_{djnj'}^{R,L}\right]=-\left[\mathbf{K}_{u1}^{-1}\mathbf{K}_{d1}-\mathbf{K}_{u2}^{-1}\mathbf{K}_{d2}\right]^{-1}\left[\mathbf{K}_{u1}^{-1}\mathbf{K}_{t1}^{R,L}-\mathbf{K}_{u2}^{-1}\mathbf{K}_{t2}^{R,L}\right],\\
&\left[L_{ujnj'}^{R,L}\right]=-\left[\mathbf{K}_{d1}^{-1}\mathbf{K}_{u1}-\mathbf{K}_{d2}^{-1}\mathbf{K}_{u2}\right]^{-1}\left[\mathbf{K}_{d1}^{-1}\mathbf{K}_{t1}^{R,L}-\mathbf{K}_{d2}^{-1}\mathbf{K}_{t2}^{R,L}\right],\\
&\mathbf{K}_{d1}=[\mathbf{D}_d^{(S-1)}\mathbf{Q}_d+\mathbf{D}_u^{(S-1)}]^{-1}\mathbf{D}_d^{(S)}\mathbf{E}_d^{(S)}(h_{t1})-[\mathbf{S}_d^{(S-1)}\mathbf{Q}_d+\mathbf{S}_u^{(S-1)}]^{-1}\mathbf{S}_d^{(S)}\mathbf{E}_d^{(S)}(h_{t1}),\\
&\mathbf{K}_{u1}=[\mathbf{D}_d^{(S-1)}\mathbf{Q}_d+\mathbf{D}_u^{(S-1)}]^{-1}\mathbf{D}_u^{(S)}\mathbf{E}_u^{(S)}(h_{t1})-[\mathbf{S}_d^{(S-1)}\mathbf{Q}_d+\mathbf{S}_u^{(S-1)}]^{-1}\mathbf{S}_u^{(S)}\mathbf{E}_u^{(S)}(h_{t1}),\\
&\mathbf{K}_{d2}=[\mathbf{D}_d^{(S+1)}\mathbf{Q}_u+\mathbf{D}_u^{(S+1)}]^{-1}\mathbf{D}_d^{(S)}\mathbf{E}_u^{(S)}(h_{t2})-[\mathbf{S}_d^{(S+1)}\mathbf{Q}_u+\mathbf{S}_u^{(S+1)}]^{-1}\mathbf{S}_d^{(S)}\mathbf{E}_u^{(S)}(h_{t2}),\\
&\mathbf{K}_{u2}=[\mathbf{D}_d^{(S+1)}\mathbf{Q}_u+\mathbf{D}_u^{(S+1)}]^{-1}\mathbf{D}_u^{(S)}\mathbf{E}_d^{(S)}(h_{t2})-[\mathbf{S}_d^{(S+1)}\mathbf{Q}_u+\mathbf{S}_u^{(S+1)}]^{-1}\mathbf{S}_u^{(S)}\mathbf{E}_d^{(S)}(h_{t2}),\\
&\mathbf{K}_{t1}^{R,L}=[\mathbf{D}_d^{(S-1)}\mathbf{Q}_d+\mathbf{D}_u^{(S-1)}]^{-1}\mathbf{D}_{ue}^{R,L}-[\mathbf{S}_d^{(S-1)}\mathbf{Q}_d+\mathbf{S}_u^{(S-1)}]^{-1}\mathbf{S}_{ue}^{R,L},\\
&\mathbf{K}_{t2}^{R,L}=[\mathbf{D}_d^{(S+1)}\mathbf{Q}_u+\mathbf{D}_u^{(S+1)}]^{-1}\mathbf{D}_{de}^{R,L}-[\mathbf{S}_d^{(S+1)}\mathbf{Q}_u+\mathbf{S}_u^{(S+1)}]^{-1}\mathbf{S}_{de}^{R,L}
\end{aligned}
\tag{10}
$$

where the expressions of the $3 \times 3(2M + 1)$ sub-matrices $\mathbf{D}_{de}^{R,L}$, $\mathbf{D}_{ue}^{R,L}$, $\mathbf{S}_{de}^{R,L}$, and $\mathbf{S}_{ue}^{R,L}$ are provided in Appendix A.

To impose the boundary conditions on the twin tunnel–soil interfaces, two problems need to be solved. Firstly, the down- and up-going plane wave functions should be expressed in the cylindrical coordinate system, which can be achieved by the following wave transformation [23]:

$$
\begin{aligned}
\hat{\tilde{\boldsymbol{\phi}}}_{dj}^{(S)}(x_R,k_y)&=\sum_{m=-N}^{N}T_{umj}^{R,L}\,\mathrm{Re}\tilde{\tilde{\boldsymbol{\chi}}}_{mj}^{R,L}(r_{R,L},\theta_{R,L}),\\
\hat{\tilde{\boldsymbol{\phi}}}_{uj}^{(S)}(x_R,k_y)&=\sum_{m=-N}^{N}T_{dmj}^{R,L}\,\mathrm{Re}\tilde{\tilde{\boldsymbol{\chi}}}_{mj}^{R,L}(r_{R,L},\theta_{R,L})
\end{aligned}
\tag{11}
$$

where the regular cylindrical wave functions $\mathrm{Re}\tilde{\tilde{\boldsymbol{\chi}}}_{mj}^{R,L}$ can easily be obtained by replacing the Hankel function $H_n^{(1)}(\cdot)$ with a Bessel function $J_n(\cdot)$ in the corresponding outgoing cylindrical wave functions.

Secondly, the cylindrical wave functions induced by the two different cavities should be expressed in the same cylindrical coordinate system. This requirement can be satisfied the addition theorem [24], [25], by which, the translation between two different cylindrical waves is given by

$$
\tilde{\tilde{\boldsymbol{\chi}}}_{nj}^{L}(r_L,\theta_L)=\sum_{m=-N}^{N}G_{nmj}^{LR}\,\mathrm{Re}\tilde{\tilde{\boldsymbol{\chi}}}_{mj}^{R}(r_R,\theta_R)
\tag{12a}
$$

$$
\tilde{\tilde{\boldsymbol{\chi}}}_{nj}^{R}(r_R,\theta_R)=\sum_{m=-N}^{N}G_{nmj}^{RL}\,\mathrm{Re}\tilde{\tilde{\boldsymbol{\chi}}}_{mj}^{L}(r_L,\theta_L)
\tag{12b}
$$

where $k_{rj}^{(S)}=k_{rs}^{(S)}$ for $j = 1, 2$ and $k_{rj}^{(S)}=k_{rp}^{(S)}$ for $j = 3$, with

$$
\begin{aligned}
G_{nmj}^{RL}&=\mathrm{e}^{-\mathrm{i}(n-m)\theta_t}H_{n-m}^{(1)}(k_{rj}^{(S)}d_t),\\
G_{nmj}^{LR}&=\mathrm{e}^{\mathrm{i}(n-m)(\pi-\theta_t)}H_{n-m}^{(1)}(k_{rj}^{(S)}d_t)
\end{aligned}
\tag{13}
$$

By substituting (11) and (12a) into (6), the displacement and stress components in the source layer L_S are expressed in the cylindrical coordinate system (r_R, θ_R, z) as:

$$
\begin{aligned}
\hat{\tilde{\mathbf{u}}}^{(S)}&=\sum_{m=-N}^{N}\sum_{j=1}^{3}\Bigg\{\frac{1}{2\pi}\int_{-\infty}^{+\infty}\mathrm{Re}\tilde{\tilde{\boldsymbol{\chi}}}_{mj}^{R}\sum_{j'=1}^{3}\sum_{n=-N}^{N}\Big[(T_{umj}^{R}L_{djnj'}^{R}+T_{dmj}^{R}L_{ujnj'}^{R})B_{nj'}^{R}\\
&\quad+(T_{umj}^{R}L_{djnj'}^{L}+T_{dmj}^{R}L_{ujnj'}^{L})B_{nj'}^{L}\Big]\mathrm{d}k_y+B_{mj}^{R}\hat{\tilde{\boldsymbol{\chi}}}_{mj}^{R}+\sum_{n=-N}^{N}B_{nj}^{L}G_{nmj}^{LR}\,\mathrm{Re}\hat{\tilde{\boldsymbol{\chi}}}_{mj}^{R}\Bigg\}\\
&=\sum_{m=-M}^{M}\mathbf{S}_m^{R}\hat{\tilde{\mathbf{U}}}_m^{R}(r_R,m,k_z,\omega),\\
\hat{\tilde{\boldsymbol{\sigma}}}^{(S)}&=\sum_{m=-N}^{N}\sum_{j=1}^{3}\Bigg\{\frac{1}{2\pi}\int_{-\infty}^{+\infty}\mathrm{Re}\hat{\tilde{\boldsymbol{\eta}}}_{mj}^{R}\sum_{j'=1}^{3}\sum_{n=-N}^{N}\Big[(T_{umj}^{R}L_{djnj'}^{R}+T_{dmj}^{R}L_{ujnj'}^{R})B_{nj'}^{R}\\
&\quad+(T_{umj}^{R}L_{djnj'}^{L}+T_{dmj}^{R}L_{ujnj'}^{L})B_{nj'}^{L}\Big]\mathrm{d}k_y+B_{mj}^{R}\hat{\tilde{\boldsymbol{\eta}}}_{mj}^{R}+\sum_{n=-N}^{N}B_{nj}^{L}G_{nmj}^{LR}\,\mathrm{Re}\hat{\tilde{\boldsymbol{\eta}}}_{mj}^{R}\Bigg\}\\
&=\sum_{m=-M}^{M}\mathbf{S}_m^{R}\hat{\tilde{\mathbf{T}}}_m^{R}(r_R,m,k_z,\omega)
\end{aligned}
\tag{14}
$$

Similarly, the combination of (6), (11), and (12b) gives the expressions of the displacement and stress components in the cylindrical coordinate system (r_L, θ_L, z):

$$
\begin{aligned}
\hat{\tilde{\mathbf{u}}}^{(S)}&=\sum_{m=-N}^{N}\sum_{j=1}^{3}\Bigg\{\frac{1}{2\pi}\int_{-\infty}^{+\infty}\mathrm{Re}\tilde{\tilde{\boldsymbol{\chi}}}_{mj}^{L}\sum_{j'=1}^{3}\sum_{n=-N}^{N}\Big[(T_{umj}^{L}L_{djnj'}^{R}+T_{dmj}^{L}L_{ujnj'}^{R})B_{nj'}^{R}\\
&\quad+(T_{umj}^{L}L_{djnj'}^{L}+T_{dmj}^{L}L_{ujnj'}^{L})B_{nj'}^{L}\Big]\mathrm{d}k_y+B_{mj}^{L}\hat{\tilde{\boldsymbol{\chi}}}_{mj}^{L}+\sum_{n=-N}^{N}B_{nj}^{R}G_{nmj}^{RL}\,\mathrm{Re}\hat{\tilde{\boldsymbol{\chi}}}_{mj}^{L}\Bigg\}\\
&=\sum_{m=-M}^{M}\mathbf{S}_m^{L}\hat{\tilde{\mathbf{U}}}_m^{L}(r_L,m,k_z,\omega),\\
\hat{\tilde{\boldsymbol{\sigma}}}^{(S)}&=\sum_{m=-M}^{M}\sum_{j=1}^{3}\Bigg\{\frac{1}{2\pi}\int_{-\infty}^{+\infty}\mathrm{Re}\hat{\tilde{\boldsymbol{\eta}}}_{mj}^{L}\sum_{j'=1}^{3}\sum_{n=-N}^{N}\Big[(T_{umj}^{L}L_{djnj'}^{R}+T_{dmj}^{L}L_{ujnj'}^{R})B_{nj'}^{R}\\
&\quad+(T_{umj}^{L}L_{djnj'}^{L}+T_{dmj}^{L}L_{ujnj'}^{L})B_{nj'}^{L}\Big]\mathrm{d}k_y+B_{mj}^{L}\hat{\tilde{\boldsymbol{\eta}}}_{mj}^{L}+\sum_{n=-N}^{N}B_{nj}^{R}G_{nmj}^{RL}\,\mathrm{Re}\hat{\tilde{\boldsymbol{\eta}}}_{mj}^{L}\Bigg\}\\
&=\sum_{m=-M}^{M}\mathbf{S}_m^{L}\hat{\tilde{\mathbf{T}}}_m^{L}(r_L,m,k_z,\omega)
\end{aligned}
\tag{15}
$$

where the regular cylindrical wave functions for stresses $\mathrm{Re}\hat{\tilde{\boldsymbol{\eta}}}_{mj}^{R,L}$ are also obtained by replacing the Hankel function $H_n^{(1)}(\cdot)$ with a Bessel function $J_n(\cdot)$ in the corresponding outgoing cylindrical wave functions. $\hat{\tilde{\mathbf{U}}}_m^{R,L}=\left[\hat{\tilde{U}}_{rm}^{R,L},\hat{\tilde{U}}_{\theta m}^{R,L},\hat{\tilde{U}}_{zm}^{R,L}\right]^{\mathrm{T}}$ and $\hat{\tilde{\mathbf{T}}}_m^{R,L}=\left[\hat{\tilde{T}}_{rrm}^{R,L},\hat{\tilde{T}}_{r\theta m}^{R,L},\hat{\tilde{T}}_{rzm}^{R,L}\right]^{\mathrm{T}}$ represent the displacement and stress components of soil in L_S, respectively, for a particular

circumferential mode m. $\mathbf{S}_m^{R,L}=\mathrm{e}^{\mathrm{i}m\theta_{R,L}}\mathbf{I}_3$, with $\mathbf{I}_3$ being the identity matrix of size 3 × 3.

The twin tunnels, which are considered as cylindrical thin shells with mean radii $a_{R,L}$ and thicknesses $h_{R,L}$, are simulated by Flügge shell equations [26] The solution for the cylindrical shell can be obtained following the derivation of the method proposed by [19], which is expressed as

$$\frac{-E_{R,L}h_{R,L}}{a_{R,L}(1-\upsilon_{R,L}^2)}\hat{\mathbf{A}}^{R,L}\left[\hat{U}_m^{R,L},\ \hat{V}_m^{R,L},\ \hat{W}_m^{R,L}\right]^{\mathrm{T}}+\left[\hat{Q}_m^{R,L},\ \hat{Q}_{\theta m}^{R,L},\ \hat{Q}_{rm}^{R,L}\right]^{\mathrm{T}}=\left[\hat{P}_{zm}^{R,L}\quad\hat{P}_{\theta m}^{R,L}\quad\hat{P}_{rm}^{R,L}\right]^{\mathrm{T}} \tag{16}$$

where $\hat{\mathbf{A}}^{R,L}$ is a 3 × 3 coefficient matrix, and the expressions of its components were given by [19]. $E_{R,L}$ and $v_{R,L}$ are Young's modulus and Poisson's ratio of the twin tunnels, respectively. $\hat{\mathbf{U}}_{tm}^{R,L}=\left[\hat{U}_m^{R,L},\hat{V}_m^{R,L},\hat{W}_m^{R,L}\right]^{\mathrm{T}}$ and $\hat{\mathbf{Q}}_{tm}^{R,L}=\left[\hat{Q}_{zm}^{R,L},\hat{Q}_{\theta m}^{R,L},\hat{Q}_{rm}^{R,L}\right]^{\mathrm{T}}$ represent the displacement and stress components for each m, respectively, while $\left[\hat{P}_{zm}^{R,L}\quad\hat{P}_{\theta m}^{R,L}\quad\hat{P}_{rm}^{R,L}\right]^{\mathrm{T}}$ represent the load components applied to the inside surface of shell. For a unit point load with a frequency f_0 and velocity v_0 is radially applied to the shell at the tunnel invert, the expression of the load is as follow:

$$\left[\hat{P}_{zm}^{R,L}\quad\hat{P}_{\theta m}^{R,L}\quad\hat{P}_{rm}^{R,L}\right]^{\mathrm{T}}=\left[0\quad 0\quad\frac{\delta(w-2\pi f_0+k_z v_0)}{a_{R,L}}e^{-\mathrm{i}m\gamma_{R,L}}\right]^{\mathrm{T}} \tag{17}$$

On the inside surfaces of the twin tunnels, the stresses are equal to the applied loads, while on the two tunnel–soil interfaces, the displacements and stresses of the soil and tunnels are continuous. Therefore, for the shell model, the combination of (16) and (17) yields the following system equation for each m:

$$\frac{-E_{R,L}h_{R,L}}{a_{R,L}(1-\upsilon_{R,L}^2)}\hat{\mathbf{A}}^{R,L}\begin{bmatrix}\hat{U}_{zm}^{R,L}\\ \hat{U}_{\theta m}^{R,L}\\ -\hat{U}_{rm}^{R,L}\end{bmatrix}_{r_{R,L}=a_{R,L}}+\begin{bmatrix}-\hat{T}_{rzm}^{R,L}\\ -\hat{T}_{r\theta m}^{R,L}\\ \hat{T}_{rrm}^{R,L}\end{bmatrix}_{r_{R,L}=a_{R,L}}=\begin{bmatrix}\hat{P}_{zm}^{R,L}\\ \hat{P}_{\theta m}^{R,L}\\ \hat{P}_{rm}^{R,L}\end{bmatrix} \tag{18}$$

The unknown coefficients $B_{mj}^{R,L}$ can be calculated by (18) and (17) along with (14) and (15) for each m. The unknown coefficients $A_{dj}^{(S)}$ and $A_{uj}^{(S)}$ in the source layer L_S are then determined from (9), while the unknown coefficients $A_{dj}^{(q)}$ and $A_{uj}^{(q)}$ for the other layers can be calculated by the transfer matrix method [16]. Once these unknown coefficients have been determined, the dynamic response at an arbitrary observation point due to the unit moving harmonic load applied to the tunnels can easily be calculated using (2) or (6) in the frequency–wavenumber domain. The results in the time-space domain can be obtained by applying the inverse Fourier transform to the solution in the frequency–wavenumber domain.

III. Numerical Results and Discussion

A. Numerical Validation

In this section, the accuracy of the proposed model is verified by means of a numerical case. Two side-by-side tunnels embedded in a three-layered half-space are considered in this case. As illustrated in Fig. 2, the two tunnels with a mean radius of 2.875 m and thickness of 0.25 m are located at a depth of 20 m in the second layer. The distance between the twin tunnels is equal to 10 m. The thicknesses of the first and second layers are 5 and 20 m, respectively. By setting the material parameters of each layer to have identical values, the three-layered half-space degenerates into a homogeneous half-space. The parameter values used to model the soil and tunnels are the same as those provided in [18].

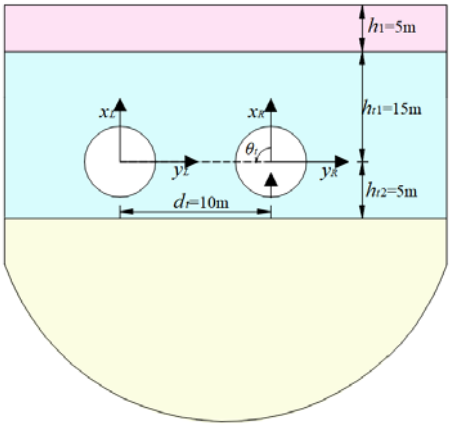

Fig. 2 Two side-by-side tunnels embedded in a three-layered half-space

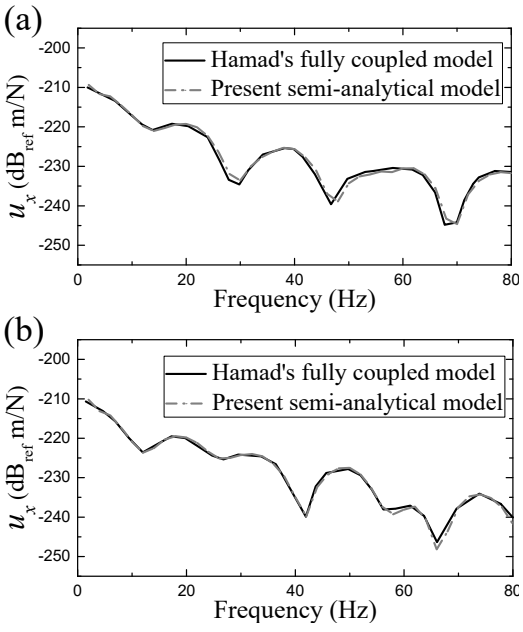

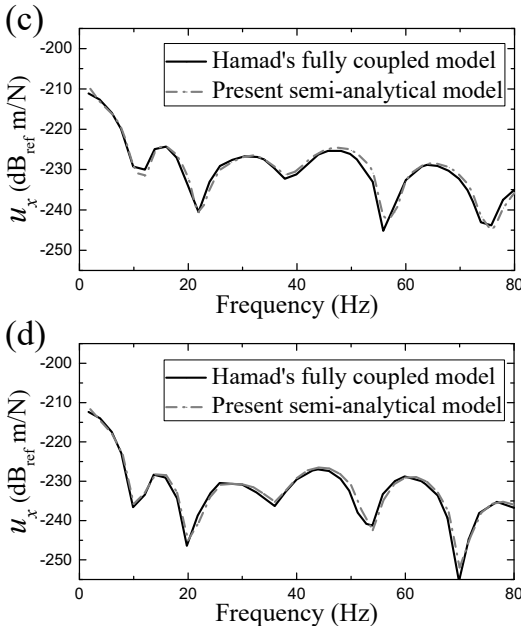

Fig. 3 Vertical displacements u_x at points (a) (x_R = 20 m, y_R = 0 m, z = 0 m), (b) (x_R = 20 m, y_R = 0 m, z = 10 m), (c) (x_R = 20 m, y_R = – 10 m, z = 0 m), and (d) (x_R = 20 m, y_R = – 10 m, z = 10 m) induced by a harmonic load applied to the base of the right-hand tunnel

Fig. 3 compares the vertical and horizontal displacements calculated by the existing fully coupled model and present analytical model at four points on the ground surface. In general, good agreements are obtained, indicating the reliable accuracy of the proposed model.

B. Effect of a Neighboring Tunnel on Ground Vibrations

In this section, the proposed model is applied to investigate effect of a neighboring tunnel on ground vibrations. As illustrated in Fig. 2, two side-by-side tunnels embedded in a three-layered half-space are considered. The twin tunnels are situated at a depth of 20 m in the second layer and separated by a distance of 10 m. The parameter values defining the properties of the tunnels and soil are presented in Tables I and II.

TABLE I
PARAMETER VALUES DEFINING THE PROPERTIES OF THE TWO TUNNELS

Young's modulus, $E_{R,L}$	5×10^{10} N/m^2
Poisson's ratio, $v_{R,L}$	0.3
Density, $\rho_{R,L}$	2500 kg/m^3
Radius, $a_{R,L}$	3 m
Thickness, $h_{R,L}$	0.25 m
Material damping ratio, β_t	0.015
Distance between two tunnels, d_t	10 m
Angle between the vector from Tunnel 1 to Tunnel 2 and x-axis, θ_t	$\pi/2$

TABLE II
PARAMETER VALUES DEFINING THE PROPERTIES OF THE SOIL

Layer thickness, h_q (m)	S-wave velocity, C_s (m/s)	P-wave velocity, C_p (m/s)	Density, ρ (kg/m^3)	Material damping ratio, β_s
5	100	200	1800	0.02
20	200	400	1800	0.02
∞	300	600	1800	0.02

A fully track model is coupled with the proposed twin–tunnel model to account for the dynamics of the track structure. As illustrated in Fig. 4, the two rails and slab are simplified as a single Euler–Bernoulli beam of infinite length. The rail pads and slab bearings are modelled as a series of springs with continuous supports. The detailed derivation process for the full track model can be found in [12]. The parameter values used to simulate the track structures that consist of a directly-fixed slab and two UIC 50 rails are summarized in Table III.

TABLE III
PARAMETER VALUES DEFINING THE PROPERTIES OF THE FULL TRACK

Bending stiffness of two rails, E_rI_r	10×10^6 Pa·m^4
Loss factor of rails in bending, η_r	0.03
Mass of two rails per unit length, m_r	100 kg/m
Normal stiffness of rail pads, k_{rp}	40×10^6 N/m^2
Loss factor of rail pads, η_{rp}	0.1
Bending stiffness of slab, E_sI_s	1.43×10^9 Pa·m^4
Mass of the slab per unit length, m_s	3500 kg/m

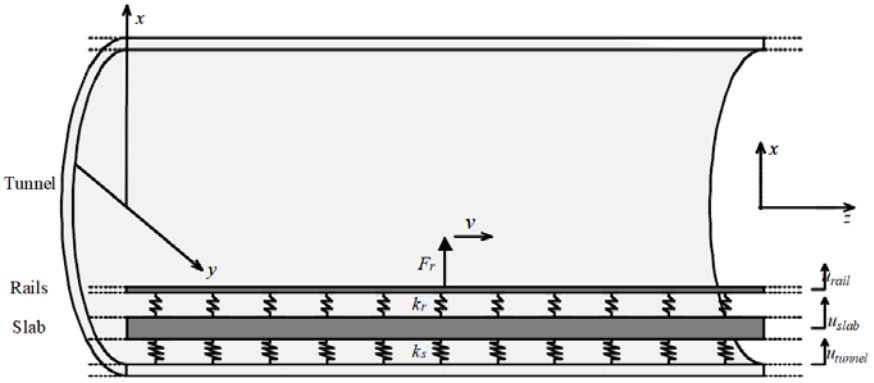

Fig. 4 Geometry of a fully track system in a circular tunnel

Fig. 5 compares the vertical displacement fields on the ground surface calculated by the single– and twin–tunnel models. The excitation is a unit, harmonic, vertical point load with a frequency of f_0 = 50 Hz. The waves generated at the rails propagate through the tunnel and soil, resulting in Rayleigh waves on the ground surface of the layered half-

space. The wave fronts on the ground surface are not cylindrical, which is a result of the dynamic interaction between the soil and tunnels. In the single–tunnel model, the vertical displacement field is symmetric about the y_R-axis. Therefore, the vertical displacement is equal in terms of both magnitude and direction. It can be observed from Fig. 5 (b) that the existence of the second tunnel disrupts this symmetry and alters the displacement field distribution, resulting in an IG of ± 20 dB.

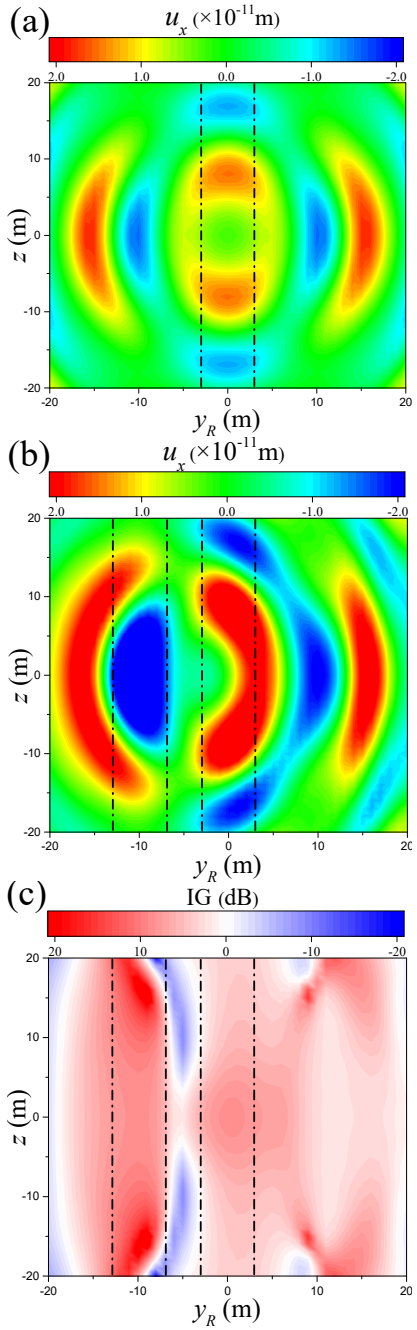

Fig. 5 Vertical displacement fields on the ground surface induced by the harmonic load with a frequency of f_0 = 50 Hz on the rails, as calculated by (a) a single–tunnel model and (b) a twin–tunnel model. The corresponding IG is shown in (c)

Fig. 6 presents the vertical displacements at four observation points on the ground surface as a function of the load frequency. It can be observed from Fig. 6 that the influence of the dynamic interaction between twin tunnels highly depends on the frequency. In the low–frequency range, the wavelength is larger than the diameter of the second tunnel, resulting in less energy being reflected by this tunnel. Therefore, the vibration levels of the single– and twin–tunnel models are similar. As the frequency increases, more energy is reflected by the second tunnel, resulting in an IG of ± 20 dB.

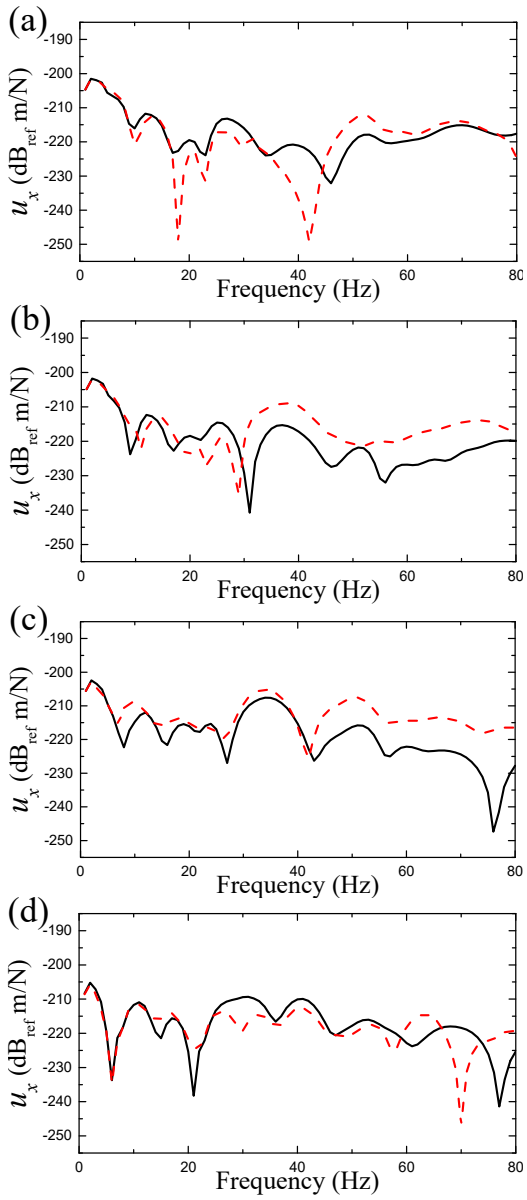

Fig. 6 Vertical displacements at points (a) (x_R = 20, y_R = 0 m, z = 0 m), (b) (x_R = 20, y_R = –5 m, z = 0 m), (c) (x_R = 20, y_R = –10 m, z = 0 m), and (d) (x_R = 20, y_R = –20 m, z = 0 m) induced by the harmonic load on the rails, as calculated by the single–tunnel model (——) and twin–tunnel model (- - -)

Next, the influence of the soil layering on the dynamic interaction between twin tunnels is investigated. Three

examples are considered by changing the shear wave velocity of one soil layer while maintaining this parameter constant for the other two layers. The shear wave velocity C_s = 200 m/s is selected as a reference. A 50% variation in the shear wave velocity is imposed to make the soil stiffer or softer.

Figs. 7-9 present the vertical displacements of the twin–tunnel model and corresponding IG values between the two tunnel models at the point (x_R = 20, y_R = –10 m, z = 0 m) for the three examples. In the low–frequency range, the vertical displacement amplitude decreases as the shear wave velocity of any soil layers increases. Since the soil response is mainly quasi–static in the low–frequency range, the soil with a higher shear wave velocity (i.e. higher stiffness) has a lower displacement amplitude. As the frequency increases, the vertical displacement curves become quite complex due to the dynamic tunnel–soil interaction.

The effect of the soil layering on the dynamic interaction between twin tunnels can also be observed in Figs. 7-9. The IG values tend to decrease as the soil stiffness increases. However, the effects of the soil stiffness of different layers on the dynamic interaction between twin tunnels are different. The stiffness of the soil above the tunnels and in which the tunnels are embedded has a significant impact on the dynamic interaction between two neighboring tunnels, while the influence of the stiffness of the soil beneath the tunnels on the dynamic interaction between twin tunnels is small.

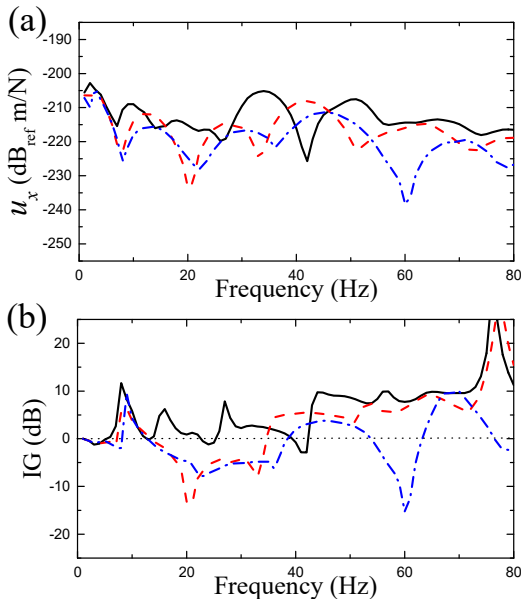

Fig. 7 (a) Vertical displacements of the twin–tunnel model and (b) corresponding IG at the point (x_R = 20, y_R = –10 m, z = 0 m) with different stiffness of the first layer: $C_s^{(1)}$ = 100 m/s (——), $C_s^{(1)}$ = 200 m/s (- - -), and $C_s^{(1)}$ = 300 m/s (—·—)

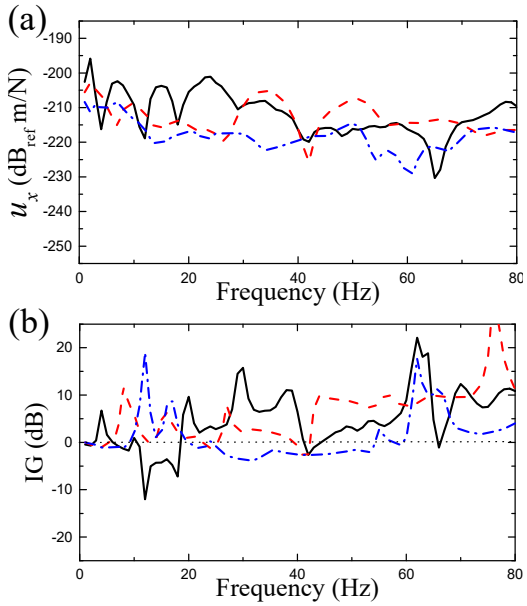

Fig. 8 (a) Vertical displacements of the twin–tunnel model and (b) corresponding IG at the point (x_R = 20, y_R = –10 m, z = 0 m) with different stiffness of the second layer: $C_s^{(2)}$ = 100 m/s (——), $C_s^{(2)}$ = 200 m/s (- - -), and $C_s^{(2)}$ = 300 m/s (—·—)

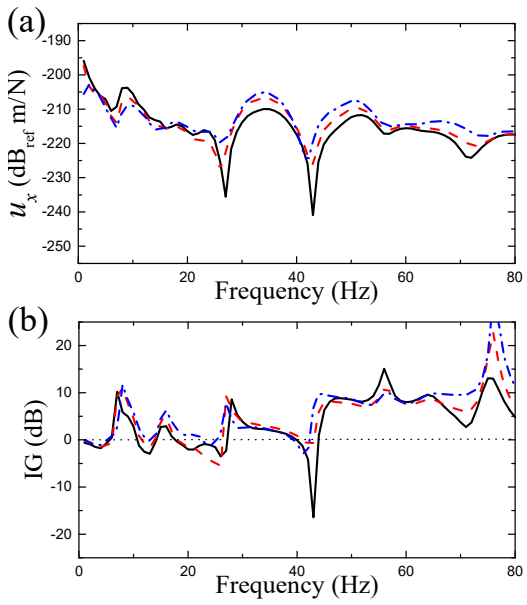

Fig. 9 (a) Vertical displacements of the twin–tunnel model and (b) corresponding IG at the point (x_R = 20, y_R = –10 m, z = 0 m) with different stiffness of the third layer: $C_s^{(3)}$ = 100 m/s (——), $C_s^{(3)}$ = 200 m/s (- - -), and $C_s^{(3)}$ = 300 m/s (—·—)

IV. Conclusions

This paper proposed a theoretical model to investigate the influence of the dynamic interaction between twin tunnels on ground vibrations. The transfer matrix method was first used to derive the relationship between the plane wave vectors in arbitrary layers and the source layer. The wave translation and transformation were then introduced to determine the plane

and cylindrical wave vectors in the source layer. By applying the compatibility of displacements and equilibrium of stresses on the two tunnel–soil interfaces, the solution for the dynamic interaction between twin tunnels in a multi-layered half-space was finally obtained.

The accuracy of the proposed model was verified by means of comparison with existing models. The train-induced vibrations from two side-by-side tunnels in a three-layered half-space were investigated. The numerical results demonstrate that the effect of the dynamic interaction between twin tunnels on the ground vibration levels, which highly depends on frequency and observation point, is significant. The stiffness of the soil above the tunnels and in which the tunnels are embedded has a significant impact on the dynamic interaction between two neighboring tunnels, while the influence of the stiffness of the soil beneath the tunnels on the dynamic interaction between twin tunnels is small.

ACKNOWLEDGEMENT

This project is supported by Projects of International Cooperation and Exchanges NSFC under grant number 51761135109, and the National Natural Science Foundation of China under grant number 51808405.

APPENDIX A

1. The sub-matrixes $\mathbf{D}_d^{(q)}$, $\mathbf{D}_u^{(q)}$, $\mathbf{S}_d^{(q)}$, $\mathbf{S}_u^{(q)}$, $\mathbf{E}_d^{(q)}$, and $\mathbf{E}_u^{(q)}$ in L_q take the forms

$$\mathbf{D}_d^{(q)}=\begin{bmatrix} D_{11}^{(q)} & D_{12}^{(q)} & D_{13}^{(q)} \\ D_{21}^{(q)} & D_{22}^{(q)} & D_{23}^{(q)} \\ D_{31}^{(q)} & D_{32}^{(q)} & D_{33}^{(q)} \end{bmatrix},\ \mathbf{D}_u^{(q)}=\begin{bmatrix} D_{11}^{(q)} & -D_{12}^{(q)} & -D_{13}^{(q)} \\ -D_{21}^{(q)} & D_{22}^{(q)} & D_{23}^{(q)} \\ D_{31}^{(q)} & D_{32}^{(q)} & D_{33}^{(q)} \end{bmatrix},$$
$$D_{11}^{(q)}=\mathrm{i}k_y,\ D_{12}^{(q)}=k_z k_{xs}^{(q)},\ D_{13}^{(q)}=-\mathrm{i}k_{xp}^{(q)},\ D_{21}^{(q)}=\mathrm{i}k_{xs}^{(q)},\ D_{22}^{(q)}=-k_z k_y,$$
$$D_{23}^{(q)}=\mathrm{i}k_y,\ D_{31}^{(q)}=0,\ D_{32}^{(q)}=k_y^2+k_{xs}^{(q)^2},\ D_{33}^{(q)}=\mathrm{i}k_z. \tag{19}$$

$$\mathbf{S}_d^{(q)}=\begin{bmatrix} S_{11}^{(q)} & S_{12}^{(q)} & S_{13}^{(q)} \\ S_{21}^{(q)} & S_{22}^{(q)} & S_{23}^{(q)} \\ S_{31}^{(q)} & S_{32}^{(q)} & S_{33}^{(q)} \end{bmatrix},\ \mathbf{S}_u^{(q)}=\begin{bmatrix} -S_{11}^{(q)} & S_{12}^{(q)} & S_{13}^{(q)} \\ S_{21}^{(q)} & -S_{22}^{(q)} & -S_{23}^{(q)} \\ S_{31}^{(q)} & -S_{32}^{(q)} & -S_{33}^{(q)} \end{bmatrix},$$
$$S_{11}^{(q)}=2\mu^{(q)}k_y k_{xs}^{(q)},\ S_{12}^{(q)}=-2\mathrm{i}\mu^{(q)}k_z k_{xs}^{(q)^2},$$
$$S_{13}^{(q)}=\mu^{(q)}(2k_p^{(q)^2}-k_s^{(q)^2}-2k_{xp}^{q)^2}),\ S_{21}^{(q)}=\mu^{(q)}(k_{xs}^{(q)^2}-k_y^2),$$
$$S_{22}^{(q)}=2\mathrm{i}\mu^{(q)}k_z k_y k_{xs}^{(q)},\ S_{23}^{(q)}=2\mu^{(q)}k_y k_{xp}^{(q)},\ S_{31}^{(q)}=-\mu^{(q)}k_z k_y,$$
$$S_{32}^{(q)}=-\mathrm{i}\mu^{(q)}k_{xs}^{(q)}(k_y^2-2k_z^2),\ S_{33}^{(q)}=2\mu^{(q)}k_z k_{xp}^{(q)}. \tag{20}$$

$$\mathbf{E}_d^{(q)}(x_{(q)})=\begin{bmatrix} \mathrm{e}^{-\mathrm{i}k_{xs}^{(q)}x_{(q)}} & 0 & 0 \\ 0 & \mathrm{e}^{-\mathrm{i}k_{xs}^{(q)}x_{(q)}} & 0 \\ 0 & 0 & \mathrm{e}^{-\mathrm{i}k_{xp}^{(q)}x_{(q)}} \end{bmatrix} \tag{21}$$

$$\mathbf{E}_u^{(q)}(x_{(q)})=\begin{bmatrix} \mathrm{e}^{\mathrm{i}k_{xs}^{(q)}x_{(q)}} & 0 & 0 \\ 0 & \mathrm{e}^{\mathrm{i}k_{xs}^{(q)}x_{(q)}} & 0 \\ 0 & 0 & \mathrm{e}^{\mathrm{i}k_{xp}^{(q)}x_{(q)}} \end{bmatrix} \tag{22}$$

2. The $3 \times 3(2M+1)$ sub-matrixes $\mathbf{D}_{de}^{R,L}$, $\mathbf{D}_{ue}^{R,L}$, $\mathbf{S}_{de}^{R,L}$, and $\mathbf{S}_{ue}^{R,L}$ take the forms

$$\begin{bmatrix} \mathbf{D}_{de}^{R,L} & \mathbf{D}_{ue}^{R,L} \\ \mathbf{S}_{de}^{R,L} & \mathbf{S}_{ue}^{R,L} \end{bmatrix}=\begin{bmatrix} \mathbf{D}_{d}^{R,L} & \mathbf{D}_{u}^{R,L} \\ \mathbf{S}_{d}^{R,L} & \mathbf{S}_{u}^{R,L} \end{bmatrix}\begin{bmatrix} \mathbf{E}_d^{R,L}(-h_{t2}) & \mathbf{0} \\ \mathbf{0} & \mathbf{E}_u^{R,L}(h_{t1}) \end{bmatrix} \tag{23}$$

with

$$\begin{cases} D_d^{R,L}(l,j+3m+3M)=D_d^{(S)}(l,j)T_{dmj}^{R,L}/k_{xj}^{(S)} \\ D_u^{R,L}(l,j+3m+3M)=D_u^{(S)}(l,j)T_{umj}^{R,L}/k_{xj}^{(S)} \\ S_d^{R,L}(l,j+3m+3M)=S_d^{(S)}(l,j)T_{dmj}^{R,L}/k_{xj}^{(S)} \\ S_u^{R,L}(l,j+3m+3M)=S_u^{(S)}(l,j)T_{umj}^{R,L}/k_{xj}^{(S)} \end{cases},\ j=l=1,2,3,\ m=-M,...,M \tag{24}$$

$$\mathbf{E}_u^{R,L}(x)=\begin{bmatrix} \mathrm{e}^{\mathrm{i}k_{xs}x} & 0 & 0 & 0 & 0 & 0 & 0 \\ 0 & \mathrm{e}^{\mathrm{i}k_{xs}x} & 0 & 0 & 0 & 0 & 0 \\ 0 & 0 & \mathrm{e}^{\mathrm{i}k_{xp}x} & 0 & 0 & 0 & 0 \\ 0 & 0 & 0 & \cdots & 0 & 0 & 0 \\ 0 & 0 & 0 & 0 & \mathrm{e}^{\mathrm{i}k_{xs}x} & 0 & 0 \\ 0 & 0 & 0 & 0 & 0 & \mathrm{e}^{\mathrm{i}k_{xs}x} & 0 \\ 0 & 0 & 0 & 0 & 0 & 0 & \mathrm{e}^{\mathrm{i}k_{xp}x} \end{bmatrix}, \tag{25}$$
$$\mathbf{E}_d^{R,L}(x)=\left[\mathbf{E}_u^{R,L}(x)\right]^{-1}$$

REFERENCES

[1] D. Clouteau, M. Arnst, T.M. Al-Hussaini, G. Degrande, Freefield vibrations due to dynamic loading on a tunnel embedded in a stratified medium, J. Sound Vib. 283 (1–2) (2005) 173–199.

[2] G. Degrande, D. Clouteau, R. Othman, M. Arnst, H. Chebli, R. Klein, P. Chatterjee, B. Janssens, A numerical model for ground-borne vibrations from underground railway traffic based on a periodic finite element–boundary element formulation, J. Sound Vib. 293(3–5) (2006) 645–666.

[3] S. Gupta, M.F.M. Hussein, G. Degrande, H.E.M. Hunt, D. Clouteau, A comparison of two numerical models for the prediction of vibrations from underground railway traffic, Soil Dynam. Earthq. Eng. 27 (7) (2007) 608–624.

[4] X. Sheng, C.J.C. Jones, D.J. Thompson, Modelling ground vibrations from railways using wavenumber finite- and boundary-element methods, Proc. Royal Soc. 461 (2005) 2043–2070.

[5] S. François, M. Schevenels, P. Galvín, G. Lombaert, G. Degrande, A 2.5D coupled FE–BE methodology for the dynamic interaction between longitudinally invariant structures and a layered halfspace, Comput. Methods Appl. Mech. Eng. 199 (2010) 1536–1548.

[6] A. Romero, P. Galvín, J. António, J. Domínguez, A. Tadeu, Modelling of acoustic and elastic wave propagation from underground structures using a 2.5D BEM-FEM approach, Eng. Anal. Bound. Elem. 76 (2017) 26–39.

[7] C. He, S.H. Zhou, H.G. Di, Y. Shan, A 2.5-D coupled FE–BE model for the dynamic interaction between saturated soil and longitudinally invariant structures, Comput. Geotech. 82 (2017) 211-222.

[8] C. He, S.H. Zhou, P.J. Guo, H.G. Di, X.H. Zhang, Modelling of ground vibration from tunnels in a poroelastic half-space using a 2.5-D FE-BE formulation, Tunn. Underg. Sp. Tech. 82 (2018) 211–221.

[9] Y.B. Yang, H.H. Hung, A 2.5D finite/infinite element approach for modelling viseo-elastic bodies subjected to moving loads, Int. J. Numer. Meth. Eng. 51(11) (2001) 1317-1336.

[10] Y.B. Yang, H.H. Hung, Soil vibrations caused by underground moving trains, J. Geotech. Geoenviron. Eng. 134 (2008) 1633–1644.

[11] J.A. Forrest, H.E.M. Hunt, A three-dimensional tunnel model for calculation of train-induced ground vibration, J. Sound Vib. 294(4–5) (2006) 678–705.

[12] J.A. Forrest, H.E.M. Hunt, Ground vibration generated by trains in underground tunnels, J. Sound Vib. 294(4–5) (2006) 706–736.

[13] M.F.M. Hussein, S. François, M. Schevenels, H.E.M. Hunt, J.P. Talbot,

G. Degrande, The fictitious force method for efficient calculation of vibration from a tunnel embedded in a multi-layered half-space, J. Sound Vib. 333 (2014) 6996–7018.
[14] H.G. Di, S.H. Zhou, C. He, X. Zhang, Z. Luo, Three-dimensional multilayer cylindrical tunnel model for calculating train-induced dynamic stress in saturated soils, Comput. Geotech. 80 (2016) 333-345.
[15] S.H. Zhou, C. He, H.G. Di, P.J. Guo, X.H. Zhang, An efficient method for predicting train-induced vibrations from a tunnel in a poroelastic half-space, Eng. Anal. Bound. Elem. 85 (2017) 43–56.
[16] C. He, S.H. Zhou, H.G. Di, P.J. Guo, J.H. Xiao, Analytical method for calculation of ground vibration from a tunnel embedded in a multi-layered half-space, Comput. Geotech. 99 (2018) 149–164.
[17] K.A. Kuo, M.F.M. Hussein, H.E.M. Hunt, The effect of a twin tunnel on the propagation of ground-borne vibration from an underground railway, J. Sound Vib. 330 (2011) 6203–6222.
[18] W. I. Hamad, H. E. M. Hunt, J. P. Talbot, M. F. M. Hussein, D. J. Thompson, The dynamic interaction of twin tunnels embedded in a homogeneous half-space, in Proceedings of the 5th ECCOMAS Thematic Conference on Computational Methods in Structural Dynamics and Earthquake Engineering, Crete Island, Greece, May 2015.
[19] C. He, S.H. Zhou, P.J. Guo, H.G. Di, X.H. Zhang, Analytical model for vibration prediction of two parallel tunnels in a full-space, J. Sound Vib. 423 (2018) 306-321.
[20] I. Sneddon, Fourier transforms. New York: McGraw-Hill; 1951.
[21] W.T. Thomson, Transmission of elastic waves through a stratified solid medium, J. Appl. Phys. 21 (1950) 89–93.
[22] N.A. Haskell, The dispersion of surface waves on multi-layered media, Bull. Seismol. Soc. Am. 43 (1953) 17–34.
[23] A. Boström, G. Kristensson, S. Ström, Transformation properties of plane, spherical and cylindrical scalar and vector wave functions, in: Varadan V.V. Lakhtakia A, V.K. Varadan (Eds.), Field Representations and Introduction to Scattering, Elsevier, Amsterdam, 1991, pp. 165–210.
[24] S.K. Bose, A.K. Mal, Longitudinal shear waves in a fiber-reinforced composite, Int. J. Solids. Struct. 9 (1973) 1075–1085.
[25] V.K. Varadan, V.V. Varadan, Y.H. Pao, Multiple scattering of elastic waves by cylinders of arbitrary cross section. I. SH waves, J. Acoust. Soc. Am. 63 (5) (1978) 1310–1319.
[26] A. Leissa, Vibration of Shells, Acoustical Society of America, New York, 1973 (reissued 1993).